J Mater Sci (2007) 42:6532–6540
DOI 10.1007/s10853-007-1552-7

# On the structure and surface properties of NiO/MgO–$La_2O_3$ catalyst: Influence of the support composition and preparation method

**Sergio L. González-Cortés · Ismael Aray · Serbia M. A. Rodulfo-Baechler · Claudio A. Lugo · Hector L. Del Castillo · Alfonso Loaiza-Gil · Freddy E. Imbert · Humberto Figueroa · Wilfredo Pernía · Alfonso Rodríguez · Oduber Delgado · Rodrigo Casanova · Juan Mendialdua · Fulgencio Rueda**

Received: 28 October 2006 / Accepted: 25 January 2007 / Published online: 30 April 2007


**Abstract** This work addresses the effect of catalyst preparation method and the carrier compositions (MgO–$La_2O_3$) over the NiO-support interaction, which affect the reducibility, textural properties and the different oxygen species chemisorbed at different temperatures over MgO–$La_2O_3$ supported NiO catalysts. The materials were prepared by wet sequential impregnation and wet co-impregnation with different Mg molar fractions [Mg/(La+Mg)]. The samples were characterized by X-ray diffraction (XRD), temperature-programmed reduction (TPR), infrared (IR) spectroscopy, scanning electron microscopy (SEM), changes of surface potential and BET surface area measurements. The total oxidation of methane was use as model reaction. It has been found that the catalyst formulations (i.e. NiO/MgO–$La_2O_3$) and the preparation methods not only affect the interaction among the catalyst components, but also the texture and material morphology as a result of different degrees of particle aggregation. The wet sequential impregnation-prepared catalysts showed a stronger MgO–$La_2O_3$ interaction than wet co-impregnation-prepared samples. A marked tendency of NiO to react with MgO rather than $La_2O_3$ following a mechanism of lattice substitution is observed. Mg-free catalyst showed $LaNiO_3$ and NiO as major crystalline Ni-containing phases. The ternary Ni–Mg–La–O system, on the other hand, facilitates the formation of poorly reducible Ni phase, whereas the La-free catalyst (i.e. NiO/MgO) displayed the lowest content of Ni-reducible phase, owing to the formation of $Ni_{1-x}Mg_xO$ solid solution. Measurements of surface potential changes together with catalytic studies suggest that La-containing catalysts present oxygen vacancies, which markedly affect the chemical nature of the surface oxygen species and hence their catalytic behaviour.

S. L. González-Cortés (✉) · I. Aray · S. M. A. Rodulfo-Baechler · C. A. Lugo · H. L. Del Castillo · A. Loaiza-Gil · F. E. Imbert · H. Figueroa · W. Pernía
Laboratorio de Cinética y Catálisis, Departamento de Química, Facultad de Ciencias, Universidad de Los Andes, La Hechicera, Merida 5101, Venezuela
e-mail: goncor@ula.ve

A. Rodríguez · O. Delgado · R. Casanova · J. Mendialdua · F. Rueda
Laboratorio de Física de Superficies, Departamento de Física, Facultad de Ciencias, Universidad de Los Andes, La Hechicera, Merida 5101, Venezuela

## Introduction

The goal of catalytic material preparation is to design a probable commercial product, which could be used as an active, selective and stable catalyst for a determined catalytic process. In order to achieve this goal, the best preparative method must be able to produce a catalytic material with appropriate textural properties (i.e., sufficiently high surface area and uniform pore distribution) and suitable mechanical strength. Supported and unsupported (or bulk) catalysts are usually thought to have an uniform chemical composition, which might present a multiphase structure as a consequence of either doping, promoting, surface or bulk segregation or even the effect of the reaction environment on the catalyst. Schwarz and co-workers [1] divided the preparation routes of catalysts into two categories: Methods in which the active phase is generated

as a solid phase by either precipitation or a decomposition reaction and methods in which the active phase is introduced and fixed onto a pre-existing solid by a process intrinsically dependent on the surface of the support. In addition, there are two main steps for the supported catalyst preparation. The first consists of depositing the active component precursor in well-divided form onto the support and the second of transforming this precursor into the required active component which, depending on the reaction to be catalyzed, can be found in the oxide, carbide, sulfide and metallic state [2].

Alkaline and rare earth oxides and their compositions have been widely used as catalysts for the oxidative coupling of methane (OCM) [3]. Among these oxides, lanthanum oxide (lanthana) and magnesium oxide (magnesia) have been also employed as supports for nickel catalysts (viz. Ni/MgO, Ni/$La_2O_3$) both for the partial oxidation of methane (POM) and for the carbon dioxide reforming of methane [4–6]. The catalysts employed for the oxidative coupling of methane are also able to catalyze the selective reduction of NOx with hydrocarbons, owing to their ability for producing methyl radicals that selectively reduce $NO_x$ [7].

Perovskite-type catalysts have been widely studied as substitutes for currently used total oxidation catalysts. Indeed, perovskite-type oxides (i.e. mixed oxides of general formula $ABO_3$, where lanthanide elements usually are at the A-site position and first row transition metals at the B-site) are less expensive and often thermally more stable than noble metals. Some formulations were found to possess similar or even higher activity than Pt-supported catalysts [8, 9]. On the other hand, the NiO/MgO and NiO/$La_2O_3$ catalysts can form either a solid solution (i.e. $Ni_{1-x}Mg_xO$) [10] or a perovskite-type phase ($LaNiO_3$) [11] upon thermal treatment, respectively. One would hence expect that their compositions (i.e. NiO/MgO–$La_2O_3$) are also active for total oxidation of methane, however, the degree of interaction of NiO with the different support components and its influence over the reducibility of nickel oxide are not easily predictable. Therefore, this work is focused on the effects of the catalyst preparation methods and the support compositions on the NiO-support interaction, which affect the reducibility, textural properties and the different oxygen species chemisorbed at different temperatures over MgO–$La_2O_3$ supported NiO catalysts. The role of various oxygen species on the total oxidation of methane was also addressed. To achieve theses aims we synthesized, using different impregnation methods, and characterized two catalyst series with variable carrier composition, keeping constant the nickel oxide loading (i.e. 19 mol.%).

## Experimental

### Sample preparation

#### *Wet sequential impregnation*

Lanthanum oxide ($La_2O_3$, Sigma 99.9%), previously calcined at 700 °C, was impregnated with an aqueous solution of magnesium nitrate-6-hydrate (E. Merck, 99%) and stirred at 70 °C for 3 h to obtain a paste with a determined molar fraction [(Mg/La+Mg)]. The solid was dried at 140 °C for 15 h and then calcined at 750 °C for 3 h in dry, $CO_2$-free air stream. Subsequently, the supports with different molar fraction were treated with nickel nitrate-6-hydrate (J.T. Baker, 99.9%) aqueous solutions to get catalysts with 19 mol.% NiO. Finally, the samples were calcined at 600 °C for 3 h in $CO_2$-free air stream and kept in a desiccator thereafter.

#### *Wet co-impregnation*

Required amounts of magnesium nitrate and nickel nitrate-6-hydrate were dissolved in distilled water and then impregnating the lanthana with a lanthana/solution ratio of 1 g/5 mL. The mixture was stirred at 70 °C for 3 h and then drying in an oven at 140 °C for 15 h. Finally, the catalysts were calcined at 600 °C for 3 h in $CO_2$-free air stream.

### Sample characterization

Semi-quantitative analysis of the catalyst series was carried out by energy-dispersive X-ray spectroscopy (EDXS) using a Kevex model Delta-3 system connected to a Hitachi model S-2500 scanning electron microscope. This instrument was also employed to find out the influence of the support composition over the catalyst morphology.

The crystalline phases of the catalysts were identified by X-ray diffraction (XRD) in a Siemens D5005 diffractometer with $\theta$:$\theta$ geometry, using CuKα radiation ($\lambda$ = 1.54059 Å) and conditions of 40 kV and 30 mA. The specimens were prepared by grinding a small amount of each sample, using an agate mortar and pestle and then loaded into a flat sample holder.

Surface areas determination is made from the adsorption isotherm, while the BET method is employed for calculation. The sample was degassed at 350 °C for 4 h, before exposing the solid to the $N_2$–He mixture.

Temperature programmed reduction (TPR) was carried out on a Micromeritics TPD/TPR 2900 system; the samples were pre-treated before analysis with a dry air flow rate of 30 mL $min^{-1}$ for 1 h at 600 °C to eliminate

adsorbed water and carbon dioxide. The TPR runs were done with a reducing $H_2$–Ar mixture (10% $H_2$), 25 mL $min^{-1}$ flow rate, 10 °C $min^{-1}$ heating rate and 50 mg of sample weight.

The IR spectra were taken in a FT-IR Perkin-Elmer 1725-X spectrometer. Approximately 1–2 mg of finely ground sample was intimately mixed with about 100 mg of dried standard infrared grade KBr using a mortar and pestle and pressed to yield a transparent disk, which was then held in a suitable holder and exposed to the infrared beam for spectroscopic examination. The analysis was carried out at room temperature under nitrogen atmosphere using 20 scans for sample and a resolution of 2 $cm^{-1}$.

Oxygen species chemisorbed on the catalyst surface were determined by measuring the surface potential changes using the vibrating capacitor technique [12]. The reference electrode was graphite, because of the inertness of this material to different gases up to 450 °C. The samples (deposited on an electrode) were previously stabilized in presence of Ar–$O_2$ mixture (oxygen partial pressure of 0.03 atm) by means of heating and cooling cycles in the temperature range of 50–450 °C, until the surface potential shows reversibility. Finally, the measurements of the capacitor potential were carried out at different oxygen partial pressures and temperatures.

### Catalytic tests

The catalytic reactions were conducted in a packed-bed tubular quartz reactor with an axial thermowell containing a chromel-alumel thermocouple centered in the catalyst bed. The sample (150 mg) was pretreated in situ at 500 °C, for 1 h with a 50 mL $min^{-1}$ dry He flow. The catalytic tests were conducted at atmospheric pressure, 500 °C, 4 vol.% $CH_4$, 5 vol.% $O_2$ in He and 30000 $h^{-1}$ of weight hour space velocity (WHSV). Gaseous products ($C_1$, $CO_2$, CO and $O_2$) separation and identification were done with an on-line gas chromatograph.

## Results and discussion

### Bulk characterization

The XRD patterns of the MgO–$La_2O_3$-supported NiO catalysts are shown in Fig. 1. Crystalline phase identification was carried out using the diffractometer analytical software after a revision of the PDF-ICDD database crystalline materials [13]. The lanthana-containing samples exhibit the characteristic peaks of lanthanum hydroxide as major phase. XRD peaks associated with lanthanum dioxomonocarbonate and perovskite-type $LaNiO_3$ phases in less extent are also observed. According to previous studies [14–16], lanthana is a basic oxide with a high tendency to adsorb water and carbon dioxide. Hence, the formation of lanthanum hydroxide is facilitated when the material is handled in humidity environment during sieving and XRD sample preparation. The presence of Mg-containing crystalline phase, on the other hand, is clearly observed when Mg molar fraction is 0.68 or 1.0. However, Ni-containing phase is not detected, likely due to the formation of $Ni_xMg_{1-x}O$ solid solution. According to Hu and Ruckenstein [5], the absence of three double peaks at 62.6°, 75.0 and 79.0 in $2\theta$ would support the solid solution formation**.** The wet co-impregnation-prepared catalysts showed a similar phase tendency than the above-mentioned samples.

In order to find out the interaction of NiO with the support components, the above catalyst series was characterized by temperature-programmed reduction (TPR). The TPR profiles are shown in Fig. 2. The catalyst free of magnesium oxide shows a complex profile with four hydrogen consumption peaks. The peaks at low reduction temperature (i.e. 272 and 305 °C) are attributed to different aggregation states of poorly-crystallized nickel oxide, since NiO was not observed by X-ray diffraction and its reduction temperature is above 300 °C [17, 18]. The peak at 350 °C is also associated with partial hydrogen consumption from the first reduction step of perovskite-type $LaNiO_3$ [18]. On the other hand, the hydrogen consumptions at higher temperatures (458 and 542 °C) are due to the last reduction step of $LaNiO_3$ and the reduction of Ni oxide species that strongly interact with structure defect of lanthana, respectively. The presence of reducible species markedly decreases with increasing MgO content. Indeed, the addition of magnesium oxide over NiO/$La_2O_3$ catalyst strongly attenuate the Ni oxide reducibility compared to Mg-free catalyst, see inset in Fig. 1, because of strong NiO–MgO interaction. This effect is significantly higher for wet co-impregnation prepared catalysts, probably due to the different contact planes available between $Ni^{2+}$ and $Mg^{2+}$ precursors that facilitate the NiO diffusion on the MgO surface during the thermal treatment. It is well-established that the reducibility of $Ni_{1-x}Mg_xO$ solid solution is very limited [6, 17], owing to the high structural stability conferred by the matrix of MgO. Therefore and in line with XRD data, the above-mentioned results support the formation of $Ni_{1-x}Mg_xO$ solid solution with increasing Mg loading. This phase would facilitate the formation of well-dispersed Ni nanoparticles over carrier with either low ability to disproportionation reaction of CO or Ni–Ni bond strength strong enough to hinder superficial reconstruction and hence coke formation upon partial oxidation of methane [19].

A schematic representation of the variation of reducible Ni phase with changing support composition is shown in

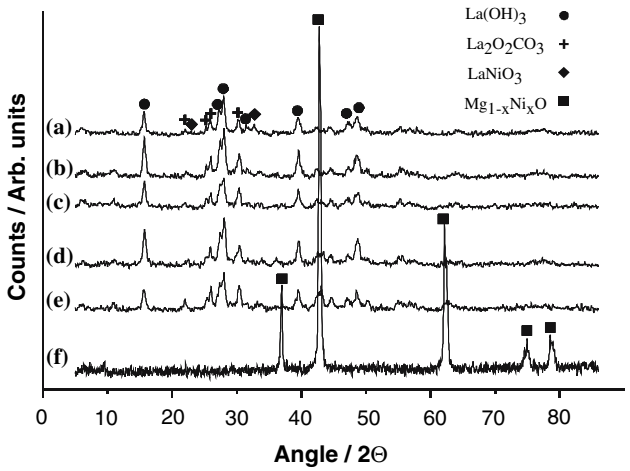


**Fig. 1** Powder XRD patterns of the 19 mol.% NiO/MgO–$La_2O_3$ catalysts prepared by wet sequential impregnation with different Mg molar fractions [i.e. Mg/(Mg+La)]. (a) 0, (b) 0.11, (c) 0.35, (d) 0.41, (e) 0.68, (f) 1.0

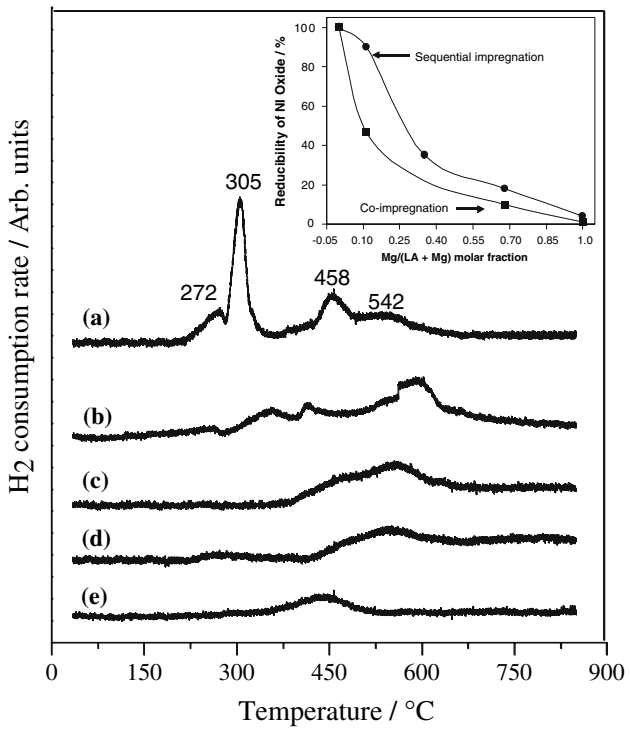


**Fig. 2** TPR profiles of the 19 mol.% NiO/MgO–$La_2O_3$ catalysts prepared by wet sequential impregnation with different Mg molar fractions. (a) 0, (b) 0.11, (c) 0.35, (d) 0.68, (e) 1.0. Inset: Influence of the Mg molar fractions over the Ni-containing phase reducibility

Fig. 3. This accounts for the marked tendency of NiO to interact with MgO rather than with $La_2O_3$ according to a mechanism of lattice substitution that leads to a system relatively homogeneous. Mg-free catalyst presented $LaNiO_3$ and NiO as major reducible Ni phases. In contrast,

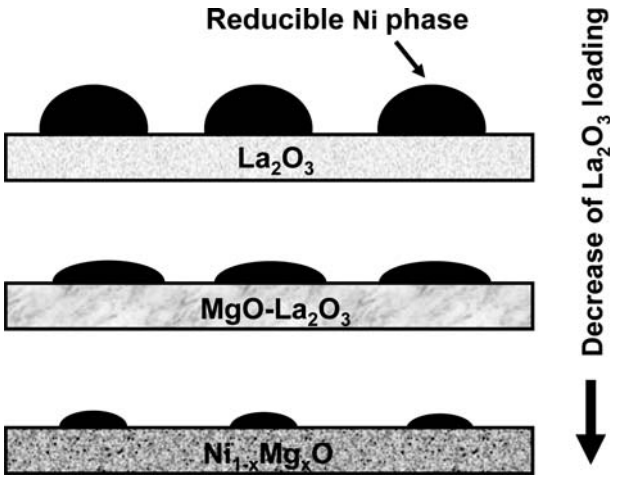


**Fig. 3** Schematic representation of MgO–$La_2O_3$-supported Ni-containing phases

the ternary Ni–Mg–La–O system facilitated the formation of less reducible Ni-containing phase, because of strong NiO–MgO interaction. The NiO/MgO catalyst, on the other hand, showed the lowest content of Ni-reducible phase, owing to the formation of bulky $Ni_{1-x}Mg_xO$ solid solution. According to Zechina et al. [20], we can assert that $Ni^{2+}$ ions preferentially diffuse to form bulk solid solution and partially occupy five-coordinated square-pyramidal sites on the (100) face of MgO and also edges (steps) and corner sites. These $Ni^{2+}$ ions located on the MgO surface are most probably reduced at temperatures higher than that of bulk NiO and below 850 °C.

The IR spectra of the MgO–$La_2O_3$-supported NiO catalysts prepared by wet sequential impregnation are shown in Fig. 4. The lanthana-containing catalysts present two bands at 1489 and 1396 $cm^{-1}$ associated with lanthanum dioxomonocarbonate ($La_2O_2CO_3$), a small peak at 856 $cm^{-1}$ corresponds to the $v_2$ mode of carbonate groups of $La_2O_2CO_3$ [21–23]. La-carbonated phases were not observed by XRD, suggesting the formation of poorly crystallized structures. According to Le van et al. [23], the strong band at 649 $cm^{-1}$ is the superposition of the $v_4$ mode of $La_2O_2CO_3$ and the $\delta_{OH}$ of the partially hydrated lanthanum oxide or $La(OH)_3$. This latter phase was also confirmed by a sharp and strong peak in the $v_{OH}$ region and by XRD. A new IR band at 424 $cm^{-1}$ for Mg molar ratio of 0.68 is defined (Fig. 4e). Indeed, this signal shows a clear shift to higher wavenumber with increasing MgO loading, reaching a maximum value at 491 $cm^{-1}$ for La-free catalyst (Fig. 4f). This band corresponds to the Mg–O stretching vibration [24], and its shift might be indicative of strong MgO–$La_2O_3$ interaction that produces local structure changes of the high cubic symmetry of MgO, since a MgO–$La_2O_3$ sample without NiO also displayed this strong

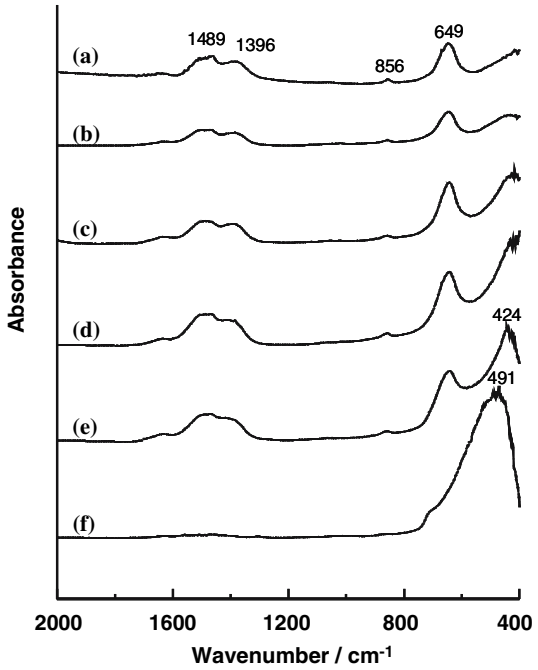


**Fig. 4** IR spectra of the 19 mol.% NiO/MgO–$La_2O_3$ catalysts prepared by wet sequential impregnation with different Mg molar fractions. (a) 0, (b) 0.11, (c) 0.35, (d) 0.41, (e) 0.68, (f) 1.0

interaction. In fact, Ivanova et al. [25] observed the formation of $La_2MgO_x$ when MgO–$La_2O_3$ is calcined at 750 °C. The IR spectra of the wet co-impregnation-prepared catalysts are shown in Fig. 5. This catalyst series shows similar spectral behaviour than that presented by above catalysts, however the wavenumber of Mg–O stretching mode for Mg molar fraction of 0.68 appears at higher wavenumber (i.e. 470 $cm^{-1}$) than that associated with the catalyst prepared by wet sequential impregnation (i.e. 424 $cm^{-1}$). This finding indicates a stronger MgO–$La_2O_3$ interaction in wet sequential impregnation-prepared catalysts because of higher thermal pretreatment of catalyst support (i.e. 750 °C). This hinders the NiO–MgO interaction relative to wet co-impregnation prepared catalysts, particularly in the catalyst with Mg molar fraction of 0.11, see inset in Fig. 2.

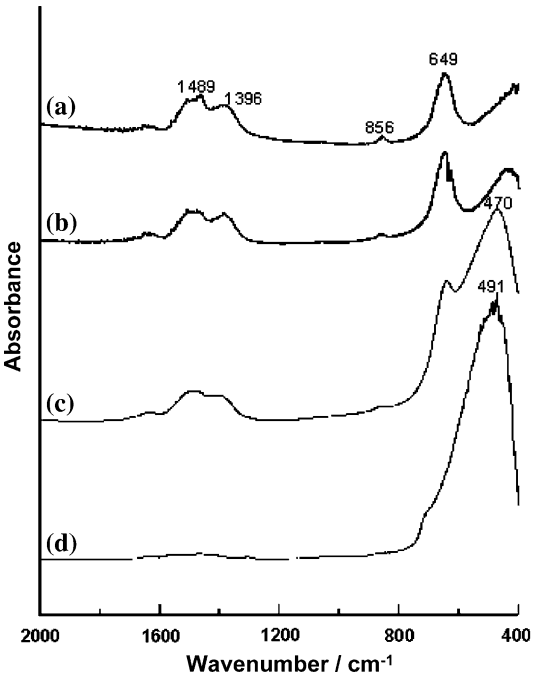


**Fig. 5** IR spectra of the 19 mol.% NiO/MgO–$La_2O_3$ catalysts prepared by wet co-impregnation with different Mg molar ratios. (a) 0, (b) 0.11, (c) 0.68, (d) 1.0

## Surface characterization

The impregnation methods employed in this work affect not only the interaction among the catalyst components, but also the textural characteristics as is illustrated in Fig. 6. Addition of small amount of MgO (9 mol.%) to NiO/$La_2O_3$ catalyst has only negligible effect on the BET specific surface area ($S_{BET}$). With increasing MgO loading, the $S_{BET}$ for wet sequential impregnation-prepared catalysts shows a maximum value for Mg molar ratio of 0.68. Further MgO content markedly decreases the $S_{BET}$. This maximum surface area is 1.5 times higher than that of NiO/$La_2O_3$ catalyst and ca. 9 times above 19 mol.% NiO/MgO catalyst. The wet co-impregnation-prepared catalysts, on the other hand, show a progressive decrease in the surface area with rising MgO content. The textural differences produced both by the preparation methods and by the Mg molar fractions over the ternary Ni–Mg–La–O system are most probably due to different aggregation degree of the catalyst particles. In fact, the SEM images in

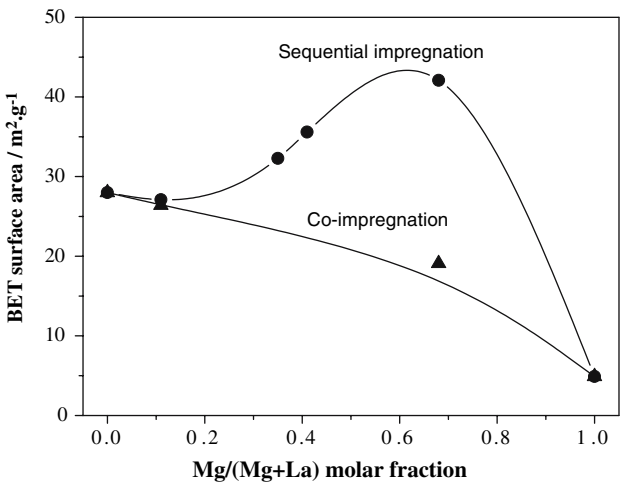


**Fig. 6** Dependence of BET specific surface area of the 19 mol.% NiO/MgO–$La_2O_3$ catalysts with variable Mg molar fractions

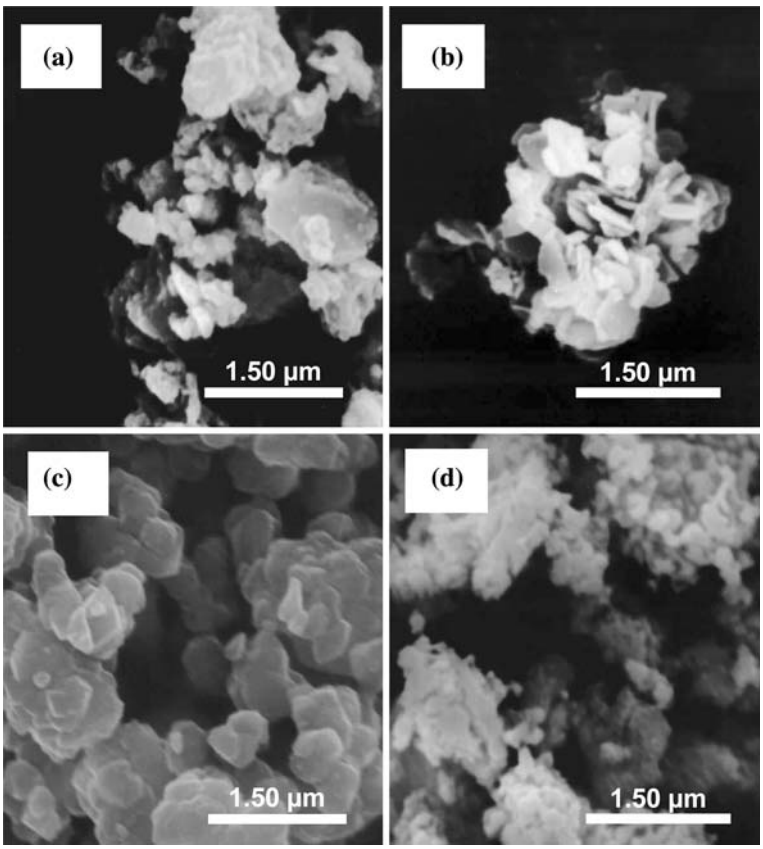


**Fig. 7** Representative SEM images of the 19 mol.% NiO/MgO–$La_2O_3$ catalysts with different Mg molar ratios. Wet sequential impregnation-prepared catalysts: (**a**) 0, (**b**) 0.68, (**c**) 1.0. Wet co-impregnation-prepared catalyst: (**d**) 0.68

Fig. 7 for wet sequential impregnation-prepared catalysts show that 19 mol.% NiO/$La_2O_3$ (Fig. 7a) has a major platelet shape morphology because of lanthana particles [23]. The Mg-enriched catalysts illustrate a flake morphology with particle soft aggregation that generates some porosity (see Fig. 7b) and particle compact aggregation that strongly decrease the total porosity (see Fig. 7c) and hence the BET surface area. On the other hand, the SEM image of wet co-impregnation-prepared catalyst reveals an agglomerated aspect with ill-defined particles, partially flat and smoother appearance (Fig. 7d). These SEM images support therefore that the preparation methods and the catalyst compositions not only affect the interaction among the catalyst components and the textural characteristics, but also the catalyst morphology as result of different particle aggregation degrees in the ternary Ni–Mg–La–O systems. A similar effect was also observed for NiO/SrO–$La_2O_3$ catalysts with support variable composition [26]. In order to find out the influence of the Mg molar ratios over the surface reactivity of the NiO/MgO–$La_2O_3$ catalysts in the oxygen adsorption reaction, in next section we determine the different oxygen species adsorbed on this catalyst series.

In Fig. 8 is displayed the kinetic studies of the oxygen adsorption monitored by measurements of the surface potential changes at 350 °C. This adsorption reaction on the catalyst surface can be described by the reaction (1):

$$\alpha O_2 + \beta e^- \longleftrightarrow N^- \tag{1}$$

where $\alpha$ and $\beta$ are non-dimensional stoichiometric coefficients and $N^-$ is the adsorbed oxygen species (i.e. $O^-$, $O^{2-}$, $O_2^-$) with the stoichiometric coefficient.

The surface potential changes (V) vs time follow the Elovich model [27], hence the data were fitted using the Eq. 2:

$$V(t) = \left(\frac{KT}{\beta e}\right) \ln\left(\frac{t}{t_o} + 1\right) \tag{2}$$

where $K$ is the Boltzman constant, $e$ the electron charge, $\beta$ the number of electrons transferred, $t$ the time on stream and $t_o$ the gas arrival time to the sample.

On other hand, the surface potential changes with partial pressure of $O_2$ ($pO_2$) are illustrated in Fig. 9, these data were fitted by using the Eq. 3:

$$V(pO_2) = \left(\frac{\alpha}{\beta}\right)\left(\frac{KT}{e}\right) \ln(pO_2) + cons\tan t \tag{3}$$

where $\alpha$ is the adsorption rate order [12].

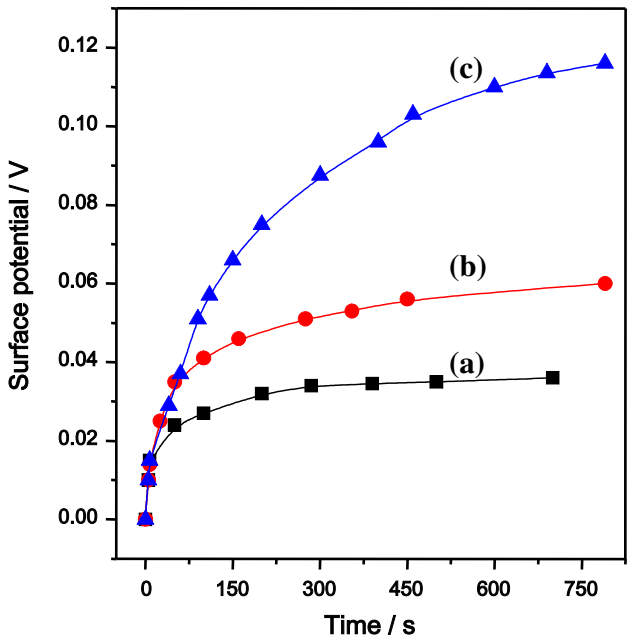


**Fig. 8** Variation of surface potential with time on stream for wet sequential impregnation-prepared 19 mol.% NiO/MgO–$La_2O_3$ catalysts. Studies conducted at 350 °C and oxygen partial pressure of 0.02 atm. (a) 0, (b) 0.68, (c) 1.0

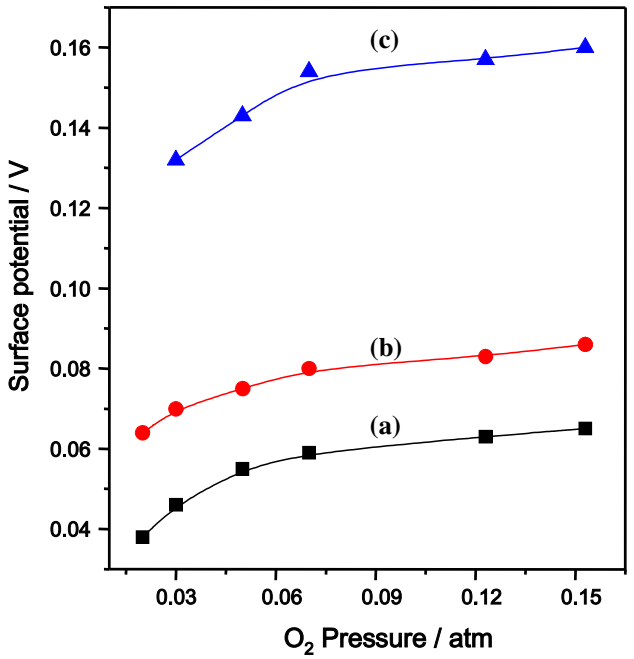


**Fig. 9** Surface potential versus oxygen partial pressure at 350 °C for wet sequential impregnation-prepared 19 mol.% NiO/MgO–$La_2O_3$ catalysts. (a) 0, (b) 0.68, (c) 1.0

All experimental data were satisfactory fitted with the above-described equations, permitting the determination of the stoichiometric coefficients (i.e. $\alpha$ and $\beta$) and hence the oxygen species adsorbed on catalyst surface, Table 1. The surface potential changes were lower for La-containing catalysts than that of 19 mol.% NiO/MgO over the whole temperature range studied. The former catalysts shows $O^-$ as major oxygen species adsorbed at 250 °C, from 350 to 425 °C a clear tendency to predominate lattice $O^{2-}$ species is noted. However, the 19 mol.% NiO/$La_2O_3$ catalyst showed a maximum surface potential of 40 mV, whereas the ternary Ni–Mg–La–O system reached ca. 65 mV (see Fig. 8). This increase indicates an improvement in the content of oxygen species as consequence of higher basicity or concentration of oxygen vacancies for NiO/MgO–$La_2O_3$ catalyst, likely due to the surface enrichment of lanthanide ions. According to XPS data, the surface of the binary Mg–La–O system was enriched in lanthana with an effective negative charge higher than that of MgO [25]. In contrast, the superoxide anion ($O_2^-$) predominates on the 19 mol.% NiO/MgO catalyst surface in the temperature range studied, reaching a maximum surface potential of approximately 130 mV. This is clearly higher than those obtained by La-containing catalysts, most probably due to an increase in the amount of oxygen chemisorbed on the catalyst surface. However, the effect of transient oxygen species with different negative charges on the surface potential measurements is not ruled out [28]. The above-discussed results indicate that the oxygen adsorption sites in La-containing catalysts have a high tendency to transfer electrons, facilitating the dissociative adsorption of dyoxygen, in contrast to La-free catalyst (NiO/MgO) that permits the adsorption of molecular oxygen.

In order to find out the ability of the ternary Ni–Mg–La–O system to transform methane to carbon dioxide, the samples were catalytically studied at 500 °C, using 4 vol.% $CH_4$ and 5 vol.% $O_2$ in He (see Fig. 10). It is clearly noticed that the support composition strongly affects not only the $CH_4$ conversion, but also the $CO_2$ selectivity. Catalysts with high La composition facilitate the formation of $CO_2$ compared with high Mg molar ratio-containing catalyst (i.e. 0.68). This tendency can be rationalized considering that different oxygen species exist at the surface as the result of the dynamic equilibrium between the metal oxide catalyst and the gas phase molecular oxygen as is illustrated in equilibrium (4) [29, 30]:

$$O_2(g) \longleftrightarrow O_2(ads) \overset{+e}{\longleftrightarrow} O_2^- \overset{+e}{\longleftrightarrow} O_2^{2-} \longleftrightarrow 2O^- \overset{+e}{\longleftrightarrow} 2O^{2-} \quad (4)$$

According to Bielański and Haber [31] the activation of hydrocarbon molecules to generate total oxidation products is driven by electrophilic oxygen species (e.g. $O_2^-$, $O^-$ and $O_{2\ (ads)}$), whereas the formation of selective oxidation products is conducted by nucleophilic lattice oxygen ions (i.e. $O^{2-}$). One can envisage that the activity-selectivity

**Table 1** Types of oxygen species on 19 mol.% NiO/MgO–$La_2O_3$ catalysts at different temperatures

| Sample [Mg/(Mg+La)] | T (°C) | $\alpha$ | $\beta$ | Oxygen species |
|---|---|---|---|---|
| NiO/$La_2O_3$ (0.0) | 250 | 1 | 2 | $O^-$ |
| | 350 | 1/2 | 2 | $O^{2-}$ |
| | 425 | 1/2 | 2 | $O^{2-}$ |
| NiO/MgO–$La_2O_3$ (0.68) | 250 | 1 | 2 | $O^-$ |
| | 350 | 1/2 | 2 | $O^{2-}$ |
| | 425 | 1/2 | 2 | $O^{2-}$ |
| NiO/MgO (1.0) | 250 | 1 | 1 | $O_2^-$ |
| | 350 | 1 | 1 | $O_2^-$ |
| | 425 | 1 | 1 | $O_2^-$ |

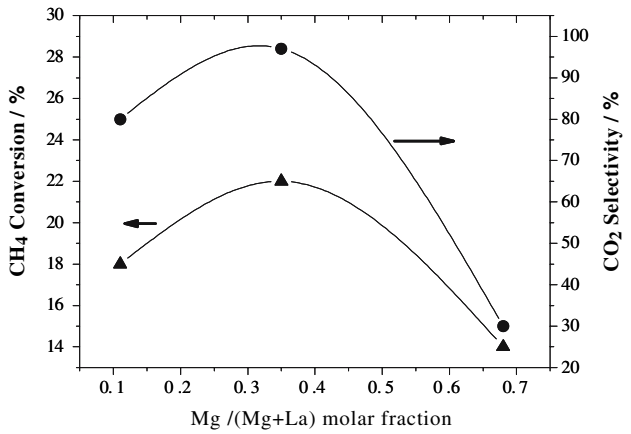


**Fig. 10** Dependence of the total oxidation of methane for the ternary Ni–Mg–La–O system with different Mg molar fractions. Catalytic reactions conducted at 500 °C, 4 vol.% $CH_4$, 5 vol.% $O_2$ in He and WHSV of 30.000 $h^{-1}$

performance of the NiO/MgO–$La_2O_3$ catalysts in the total oxidation of methane is likely associated with the equilibrium (5) [32]:

$$O_o^{2-} \leftrightarrow V_o^- + O_{Chem}^- \quad (5)$$

Which reveals that the concentrations of electrophilic and nucleophilic oxygen species depend upon the abundance of oxygen vacancies (i.e. $V_o^-$) [33]. The above-mentioned propose is based on the presence of a strong MgO–$La_2O_3$ interaction in the NiO/MgO–$La_2O_3$ catalysts, particularly in the sample with Mg molar ratio of 0.68. This interaction might facilitate the formation of oxygen vacancies, which decrease the concentration of transient electrophilic oxygen ions, compared with catalysts with lower Mg molar fractions, and hence the methane conversion and $CO_2$ selectivity (see Fig. 10).

With the support of the experimental observations, a probable sequential reaction pathway is suggested. Hydrogen abstraction from $CH_4$ occurs at the surface electrophilic oxygen sites, leading to the formation of methoxide anion [31] continued by electrophilic (or nucleophilic) oxygen insertion and/or hydrogen abstraction that end in total oxidation products (i.e. $H_2O$ and carbon dioxides), see reaction (6):

$$CH_4 \longrightarrow [O^-]CH_3O \longrightarrow [O^-]CO + CO_2 + H_2O \quad (6)$$

Catalytic species regeneration occurs by elimination of $H_2O$ and concomitant formation of electrophilic oxygen sites. The tendency to form CO or $CO_2$ as main oxidation product is probably associated not only with the different oxidizing ability of the electrophilic oxygen species involved upon the catalytic reaction, but also with the enhanced reaction rate of the electrophilic-to-nucleophilic oxygen transition by the presence of oxygen vacancies.

## Conclusions

The wet sequential impregnation-prepared catalysts show a stronger MgO–$La_2O_3$ interaction than wet co-impregnation-prepared catalysts, owing to the higher thermal pre-treatment of catalyst support. A marked tendency of NiO to react with MgO rather than with $La_2O_3$ following a mechanism of lattice substitution is observed. The catalyst with 19 mol.% NiO/$La_2O_3$ showed $LaNiO_3$ and NiO as major crystalline and reducible Ni-containing phases. The ternary Ni–Mg–La–O system, on the other hand, facilitates the formation of poorly reducible Ni phases, because of strong NiO–MgO interaction. La-free catalyst (i.e. NiO/MgO) displayed the lowest content of Ni-reducible phase, due to the formation of bulky $Ni_{1-x}Mg_xO$ solid solution. It is proposed that $Ni^{2+}$ ions partially occupy surfaces sites of MgO are reduced at temperatures above bulky NiO.

The catalyst formulations (i.e. NiO/MgO–$La_2O_3$) and the preparation methods not only affect the interaction among the catalyst components, but also the texture and catalyst morphology as result of different degrees of particle

aggregation, particularly in the ternary Ni–Mg–La–O system. Measurements of surface potentials reveal that La-containing catalysts present oxygen vacancies that facilitate the dissociative adsorption of dyoxygen to lattice $O^{2-}$ ions. On the other hand, La-free catalyst (i.e. 19 mol.% NiO/MgO) permits the adsorption of molecular oxygen to form $O_2^-$ ions. The La-enriched catalysts favour the formation of carbon dioxide whereas the Mg-enriched catalyst (i.e. Mg molar fraction of 0.68) facilitated the production of carbon monoxide from the methane oxidation reaction. This different catalytic behaviour is tentatively attributed not only to different oxidizing ability of the electrophilic oxygen species involved upon the catalytic reaction, but also to the presence of oxygen vacancies that enhance the rate of the electrophilic-to-nucleophilic oxygen transition.

**Acknowledgement** This work was financially supported by FONACIT (project No. S1-2000000814). I.A., C.A.L., H.F., W.P. and O.D. thank to CDCHT for funding.

## References

1. Scharz JA, Contescu C, Contescu A (1995) Chem Rev 95:477
2. Che M, Clause O, Marcilly Ch (1999) In: Preparation of solid catalysts, Gerhard E, Knozinger H, Helmut W (eds) Wiley-VCH, Weinheim, p 315
3. Amenomiya Y, Birss VI, Goledzinowski M, Galuska J, Sanger AR (1990) Catal Rev-Sci Eng 32:163
4. Zhang Z, Verykios XE, J Chem Soc, Chem Commun (1995) 71
5. Hu Y-H, Ruckenstein E (1997) Catal Lett 43:71
6. Requies J, Cabrero MA, Barrio VL, Güemez MB, Cambra JF, Arias PL, Pérez-Alonso FJ, Ojeda M, Pena MA, Fierro JLG (2005) Appl Catal A:Gen 289:214
7. Zhang X, Walters AB, Vannice MA (1994) J Catal 146:568
8. Arai H, Yamada T, Eguchi K, Seiyama T (1986) Appl Catal 26:265
9. Klvana D, Kirchnerova J, Chaouki J, Delval J, Yaïci W (1999) Catal Today 47:115
10. Arena F, Horrell BA, Cocke DL, Parmaliana A, Giordano N (1991) J Catal 132:58
11. González-Cortés SL, Fontal B, Moronta D (2001) Rev Mex Fis 47:367
12. Libre JM, Barbaux Y, Grzybowska B, Bonnelle JP (1981) React Kinet Catal Lett 20:249
13. JCPDS Powder Diffraction File (1989) Internacional Centre for Diffraction Data, Swarthmore, PA
14. Bernal S, Botana FJ, García R, Rodríguez-Izquierdo JM (1983) Thermochim Acta 83:139
15. Bernal S, Diaz JA, García R, Rodríguez-Izquierdo JM (1985) J Mater Sci 20:537
16. Squire GD, Luc H, Puxley DC (1994) Appl Catal A:Gen 108:261
17. Parmaliana A, Arenas F, Frusteri F, Giordano N (1990) J Chem Soc Faraday Trans 86:2663
18. González-Cortés SL, Orozco J, Fontal B (2001) Appl Catal A:Gen 213:259
19. Tsang S, Lin J, Tan KL (1998) Catal Lett 51:169
20. Zechina A, Spoto G, Coluccia S, Guglielminotti E (1984) J Chem Soc Faraday Trans 80:1875
21. Turcotte RP, Sawyer JO, Eyring L (1968) Inorg Chem 8:238
22. Taylor RP, Schrader GL (1991) Ind Eng Chem Res 30:1016
23. Le Van T, Che M, Tatibouët JM, Kermarec M (1993) J Catal 142:18
24. Kuz'mitskaya SY, Odegova GV, Vasil'eva NA, Plyasova LM, Kriger TA, Zaikovskii VI (1997) Kinet Catal 38:848
25. Ivanova AS, Moroz BL, Moroz EM, Larichev YV, Paukshtis EA, Bukhtiyarov VI (2005) J Solid State Chem 178:2365
26. Rodulfo-Baechler SMA, Pernía W, Aray I, Figueroa H, González-Cortés SL (2006) Catal Lett 112:231
27. Taylor HA, Thon N (1952) J Am Chem Soc 74:4169
28. Courcot D, Grzybowska B, Barbaux Y, Rigole M, Pochel A, Guelton M (1996) J Chem Soc, Faraday Trans 92:1609
29. Shevts VA, Vrotyntsev VM, Kazansky VB (1969) Kinet Catal 10:356
30. Kazansky VB (1977) Kinet Catal 18:43
31. Bielański A, Haber J (1991) In: Oxygen in catalysis, Marcel Dekker, Inn
32. Haber J, Turek W (2000) J Catal 190:320
33. Sokolovskii VD (1990) Catal Rev-Sci Eng 32:1